A turbulent combustion model for soot formation at the LES subgrid-scale using virtual chemistry approach

Hernando Maldonado Colmán, Nasser Darabiha, Denis Veynante, Benoit Fiorina

A turbulent combustion model for soot formation at the LES subgrid-scale using virtual chemistry approach

Hernando Maldonado Colmán[a,*], Nasser Darabiha[a], Denis Veynante[a], Benoît Fiorina[a]

[a] *Université Paris-Saclay, CNRS, CentraleSupélec, Laboratoire EM2C, 91190, Gif-sur-Yvette, France*

Abstract

Designing efficient and clean combustion devices to reduce soot formation in practical applications is a major concern nowadays. This could be achieved by performing predictive simulations in turbulent sooting combustors. Large Eddy Simulation (LES) is an attractive approach to predict flame/turbulence interactions at small scales including soot phenomena. However, because of the peculiarly complex nature of soot production phenomena, turbulent sooting flames remain very difficult to simulate and are computationally expensive. Thus, reduced gas-phase kinetics and soot models should be included in numerical simulations. The reduced virtual chemistry approach is a great alternative to address this problem since it introduces an optimized and flexible strategy to tackle multi-mode turbulent combustion and pollutants prediction. Also, the virtual chemistry approach has recently demonstrated its capability in reproducing soot phenomena in laminar flames including radiative heat transfer. In the present work, the virtual chemistry methodology

*Corresponding author. Current affiliation: Department of Mechanical and Aerospace Engineering, Princeton University, Princeton, NJ 08544, USA

Email address: hm2524@princeton.edu (Hernando Maldonado Colmán)

is extended to resolve turbulent sooting flames using LES. Based on analysis of flame and soot chemical time scales along with turbulent time scale, an original hybrid turbulent combustion model formulation is proposed, which degenerates to the flamelet regime in the flame front region and to a PSR formalism in the post-flame zone, characterized by slow soot chemistry. The subgrid-scale model for turbulence-chemistry-soot interactions is then implemented in an LES framework. The model is challenged in the turbulent non-premixed sooting flame from Sandia Laboratory. Results indicate that the LES subgrid-scale model has a significant impact on soot formation and confirms previous observations from the literature in LES of non-premixed turbulent sooting flames. Additionally, results show that the virtual chemistry can reproduce flame-soot characteristics of a turbulent sooting jet flame and are comparable to other state-of-the-art works.
Keywords:
Soot; Turbulent flames; Soot subgrid-scale model; Virtual chemistry

1. Introduction

Soot modeling in turbulent flames is a great challenge because of the complexity of multi-physical phenomena involved. The numerical modeling strategy must tackle the complexity of the chemical process involved in the soot formation along with the interactions with the turbulence.

The gas-phase kinetics must reproduce not only the flame structure but also recover small hydrocarbon radicals as well as soot precursors and polycyclic aromatic hydrocarbons (PAHs) [1]. The prediction of these species needs the knowledge of the complex chemical pathways described using de-

tailed mechanisms involving hundreds of species and thousands of reactions. These mechanisms require prohibitive CPU times to be used in LES of practical applications. Consequently, kinetic reduction techniques such as tabulated methods [2, 3], analytically reduced chemistry approaches [4] and global optimized chemistry [5] have been developed. In particular, a reduced chemistry method based on the virtual chemistry concept has recently been proposed by Maldonado Colmán *et al.* [6] to predict the soot volume fraction at very low CPU cost. This new approach accounts for a "soot chemistry" representation that envelops both soot particle dynamics and soot surface reactivity [6].

Coupling detailed soot chemistry with the turbulence is a key modeling challenge [7]. In LES, a number of developments have been proposed on subgrid-scale closures of the filtered soot source terms [7–10] and typically assume the same turbulence-flame interaction regime for all chemical species. However, the wide range of chemical time and length scales covered by detailed soot chemistry complicates the subgrid-scale (SGS) modeling of soot formation. Indeed, turbulent combustion models are generally valid in a specific flame regime identified in the Borghi diagram [11]. For instance, models based on geometrical approach [12] are well adapted to the flamelet regime where the chemistry is much faster than the flow. At the opposite, when the chemistry is slow, the reactive layer is distributed, and PSR-like models are more appropriate to LES modeling [13, 14]. The issue is therefore that interactions between turbulence and soot chemistry are expected to cover both flamelet and distributed regimes in the Borghi diagram. In the LES context, statistical PDF models which are independent of the turbulent combustion

regime can be used to model turbulence-chemistry interactions. Examples of PDF models are found in recent works of Huo *et al.* [15], introducing a Multiple Mapping Conditioning for LES (MMC-LES) coupled to a detailed sectional kinetic scheme, and that of Sun and Rigopoulos [16], proposing a new methodology that includes the Population Balance Equation (PBE) of soot particles into the LES-PDF of the gas phase. Although both groups have successfully reproduced laboratory-scale turbulent sooting flames, these approaches are rather computationally expensive to simulate large-scale industrial applications [12]. Therefore, a better alternative would be to keep a geometric approach, which reduces computational costs, but extends its validity to the PSR regime.

The objective of the present paper is to develop a turbulent combustion model for soot formation. Chemical kinetics will be based on the virtual chemistry methodology recently extended to soot [6] and validated on laminar flame configurations. An original hybrid turbulent combustion model formulation is proposed, which degenerates to the flamelet regime in the flame front region and to a PSR formalism in the post-flame zone, characterized by slow soot chemistry. Then, the model is challenged in the turbulent non-premixed sooting flame from Sandia [17], in which the SGS model has a significant impact on soot formation [7].

In the present work, the LES formalism for mass fraction filtered transport equations is first presented in Section 2. Section 3 briefly introduces the fundamentals of the virtual chemistry methodology. Section 4 expands the virtual chemistry approach to an LES framework for turbulent combustion and presents the derivation of a new hybrid SGS model for turbulence-chemistry-

soot interactions. The new hybrid SGS model for virtual chemistry is then applied to a laboratory-scale turbulent sooting flame. The experimental and LES numerical setups are described in Section 5. Finally, in Section 6, results using the new hybrid model is challenged to experimental measurements, as well as other numerical results found in the literature.

2. LES formalism: Mass fraction filtered transport equations

By employing the Thickened Flame model for LES (TFLES), the Favre-filtered transport equation of the k^{th} species mass fraction Y_k is typically expressed as:

$$\frac{\partial \bar{\rho}\widetilde{Y}_k}{\partial t} + \frac{\partial}{\partial x_i}\left(\overline{\rho u}_i \widetilde{Y}_k\right) = \frac{\partial}{\partial x_i}\left[\left(F_T \Xi_\Delta \frac{\mu}{\mathrm{Sc}_k} + (1-S_F)\frac{\mu_t}{\mathrm{Sc}_{t,k}}\right)\frac{\partial \widetilde{Y}_k}{\partial x_i}\right] + \overline{\dot{\omega}}_k, \tag{1}$$

where ρ is the mixture density and u_i is the i^{th} component of the velocity. μ and μ_t are the laminar and turbulent viscosity, respectively. $\mathrm{Sc_k}$ and $\mathrm{Sc}_{t,k}$ are respectively the k^{th} species laminar and turbulent Schmidt numbers. Ξ_Δ is the subgrid flame wrinkling. Dynamic thickening [18] is applied by using the flame sensor:

$$S_F = \max(S_{F,k}, 0),$$

where $S_{F,k}$ is defined equal to 1 within the k^{th} species reactive layer and 0 outside [19]. The thickening factor is $F_T = \max(F_{T,k}, 1)$, with:

$$F_{T,k} = \max\left[1 + (F_{T,k}^{\max} - 1)S_{F,k}, 1\right]. \tag{2}$$

Naturally, the TFLES model considers the flame front region ($S_F = 1$) to be in the flamelet regime [20] and therefore the diffusive term outside the flame,

hereafter referred as the post-flame region, includes a turbulent diffusive contribution. Further analyses in the following sections require a more explicit notation in terms of these two regions, and therefore, Eq. 1 is rewritten as follows:

$$\frac{\partial \bar{\rho}\widetilde{Y}_k}{\partial t} + \frac{\partial}{\partial x_i}\left(\overline{\rho u}_i \widetilde{Y}_k\right) = \frac{\partial}{\partial x_i}\left(S_F F_T \Xi_\Delta \frac{\mu}{\mathrm{Sc}_k}\frac{\partial \widetilde{Y}_k}{\partial x_i}\right) + \frac{\partial}{\partial x_i}\left[(1-S_F)\left(F_T \Xi_\Delta \frac{\mu}{\mathrm{Sc}_k} + \frac{\mu_t}{\mathrm{Sc}_{t,k}}\right)\frac{\partial \widetilde{Y}_k}{\partial x_i}\right] + \overline{\dot{\omega}}_k, \tag{3}$$

where the first term in the RHS corresponds exclusively to the flame front region ($S_F = 1$) and the second one to the post-flame region ($S_F = 1$). Now, note that when $S_F = 0$, following Eq. 2, $F_T \Xi_\Delta = 1$. One then can write:

$$\frac{\partial \bar{\rho}\widetilde{Y}_k}{\partial t} + \frac{\partial}{\partial x_i}\left(\overline{\rho u}_i \widetilde{Y}_k\right) = \frac{\partial}{\partial x_i}\left(S_F F_T \Xi_\Delta \frac{\mu}{\mathrm{Sc}_k}\frac{\partial \widetilde{Y}_k}{\partial x_i}\right) + \frac{\partial}{\partial x_i}\left[(1-S_F)\left(\frac{\mu}{\mathrm{Sc}_k} + \frac{\mu_t}{\mathrm{Sc}_{t,k}}\right)\frac{\partial \widetilde{Y}_k}{\partial x_i}\right] + \overline{\dot{\omega}}_k, \tag{4}$$

3. Soot virtual chemistry modeling

A virtual chemical scheme consists of virtual species and reactions whose thermo-chemical properties are optimized by machine learning algorithms [21]. The range of application of reduced virtual schemes is given by the operating conditions and flame configurations covered by the learning database [22]. The virtual chemistry model is composed of a main scheme, dedicated to capture heat release and temperature, and one or more satellite sub-mechanisms devoted to pollutant prediction such as CO [22], NO_x [23] or soot [6]. In the present study, the main mechanism for ethylene-air combustion from [6] is retained:

$$\alpha^M_{F,1}F + \alpha^M_{Ox,1}Ox \rightarrow \alpha^M_{I,1}I \qquad (R^M_1)$$

$$I \rightarrow \sum_{k=1}^{N_P^M} \alpha^M_{P_{k,2}} P_k \qquad (R^M_2)$$

Also, the following virtual soot sub-mechanism proposed in [6] is employed:

$$\alpha^s_{F,1}F + \alpha^s_{Ox,1}Ox \rightarrow \alpha^s_{V_1,1}V_1 + \alpha^s_{V_3,1}V_3 \qquad (R^s_1)$$

$$V_1 \rightarrow \alpha^s_{\mathcal{S},2}\mathcal{S} + \alpha^s_{V_2,2}V_2 \qquad (R^s_2)$$

$$\mathcal{S} + V_1 + V_2 \rightarrow \alpha^s_{\mathcal{S},3}\mathcal{S} + \alpha^s_{V_3,3}V_3 \qquad (R^s_3)$$

$$\mathcal{S} + Ox + V_2 \rightarrow Ox + 2V_3 \qquad (R^s_4)$$

In these reactions, F and Ox correspond to the fuel and oxidizer respectively. I, P_k , V_1, V_2 and V_3 are virtual species. Analysis conducted in [21] showed that an accurate prediction of equilibrium flame temperature over the whole range of equivalence ratios is obtained with four products, $N_P^M = 4$. The virtual species $\mathcal{S}$ corresponds to soot. $\alpha^M_{k,r}$ and $\alpha^s_{k,r}$ are stoichiometric coefficients per unit mass of the k^{th} virtual species in the r^{th} virtual reaction,

where the superscript M and s respectively correspond to the main and soot sub-mechanism. The soot volume fraction is obtained from $f_v^s = \rho Y_{\mathcal{S}}^s/\rho_s$ where the soot mass fraction $Y_{\mathcal{S}}^s$ is tracked by the virtual species $\mathcal{S}$. The soot density ρ_s is set to 1800 kg m^{-3}. The rate of progress of the r^{th} virtual reaction in a mechanism v (M or s) is modeled by the Arrhenius law:

$$q_r^v = A_r^v \cdot T^{\beta_r^v} \ \exp\left(\frac{E_{a,r}^v}{RT}\right) \ \prod_{k=1}^{N_s^v} [\psi_k^v]^{n_{k,r}^v}, \tag{5}$$

where N_s^v is the number of virtual species in mechanism v. A_r^v, β_r^v, $E_{a,r}^v$ and $n_{k,r}^v$ are kinetics constants optimized by a machine learning algorithm. $[\psi_k^v]$ denotes the molar concentration of the virtual species ψ_k^v. To ensure consistency between the main and soot mechanisms, $\alpha_{F,1}^s = \alpha_{F,1}^M$, $\alpha_{Ox,1}^s = \alpha_{Ox,1}^M$, and kinetics rate parameters of reactions R_1^M and R_1^s are identical. The chemical source term of the k^{th} virtual species in mechanism v is then given by:

$$\dot{\omega}_k^v = \sum_{r=1}^{N_r^v} \alpha_{k,r}^v q_r^v \tag{6}$$

where N_r^v is the number of reactions in mechanism v.

Virtual main and soot mechanisms have been optimized in [6] to target an ensemble of reference flame solutions computed using the CRECK detailed mechanism [24], including 297 species and 16797 reactions.

To optimize the main mechanism, a learning database made of 26 premixed flames with equivalence ratios ϕ in the range $[0.5; 3.0]$ is used. As explained in [6], the soot sub-mechanism is optimized on a different database made of 11 premixed flames with $\phi \in [1.8; 2.8]$ and 6 non-premixed flames of strain rates $a \in \{6, 10, 25, 45, 60, 90\}$ s^{-1}. The virtual soot sub-mechanism

reproduces faithfully the soot volume fraction given by detailed chemistry simulations in both premixed and non-premixed radiative laminar flames [6].

4. Soot turbulent modeling

4.1. Chemical time and length scales

The modeling of filtered chemical reaction rates $\overline{\dot{\omega}}_k^v$ should consider the regime of interactions between chemistry and turbulence. In most cases, chemical phenomena responsible of heat release exhibit time scales much shorter than that of turbulence. Filtered chemical reaction rates of thickened species involved in the main mechanism are then usually modeled under the flamelet regime assumption [20]. However this hypothesis is questionable for soot chemistry which exhibits a broader range of characteristic time scales.

To evidence this issue, a 1-D freely-propagating premixed ethylene-air flame calculated using the virtual chemistry model including radiative effects [6] for a rich mixture of equivalence ratio of $\phi = 2.4$ is analyzed here. Figure 1(top) presents a sample of thermochemical quantities corresponding to the main mechanism: the temperature (T), an intermediate virtual species (I) and one virtual product (P_1). Quantities of P_2, P_3 and P_4 are similar to those of P_1 and therefore are not shown. In the left column, all quantities evolve within the thermal flame thickness, $\delta_L^0 = (T_{\max} - T_{\min})/\max(dT/dx)$, here of the order of $\delta_L^0 \approx 1$ mm. All quantities in Fig. 1, except for the temperature, are normalized by their maximum value and are indicated by the operator $\langle \cdot \rangle$.

Chemical species involved in the soot sub-mechanism are presented in Fig. 1, with a focus on the thermal layer (middle) and the post-flame region

(bottom). Quantities V_3 are similar to those of V_1 and consequently is not plotted. As the species I in the main mechanism, the intermediate species V_1, directly linked to the consumption of F and Ox through reaction R_1^s is produced within the flame front. However, this is not the case of virtual species involved in R_2^s to R_4^s, such as $\mathcal{S}$ or V_2, which are mainly produced and consumed in the post-flame region (see bottom subfigures). The thickness of the soot reactive layer δ^0_{soot} is defined by the zone where $|\dot{\omega}^s_{\mathcal{S}}| > 0.001\times$ $\max(|\dot{\omega}^s_{\mathcal{S}}|)$. For $\phi = 2.4$, $\delta^0_{\text{soot}} \approx 100$mm which is much higher than δ^0_L. Thus, the soot species cannot be localized by the flame sensor.

Chemical time scales τ_c^M and τ_c^s, representative of the main and soot virtual mechanisms, respectively, are now introduced as:

$$\tau_c^M = \frac{\delta^0_L}{S^0_{fg}}, \quad \tau_c^s = \frac{\delta^0_{\text{soot}}}{S^0_{bg}}, \tag{7}$$

where S^0_{fg} and S^0_{bg} are the flame displacement speeds in the fresh and burnt gases, respectively [20]. These chemical time scales associated with the flame front and the soot formation are plotted as a function of the equivalence ratio in Fig. 2. As the chemical characteristic time of soot formation is about three orders of magnitude slower than that of the main chemical species, interactions with the turbulence will therefore be different. Nevertheless, it should be noted that other chemical species of the soot sub-mechanism, such as V_1 and V_3, are also interacting in the flame front region as mentioned before (see Fig. 1), and consequently turbulence-chemistry interactions of such species belong to multiple regimes and further measures must be taken in the post-flame region.

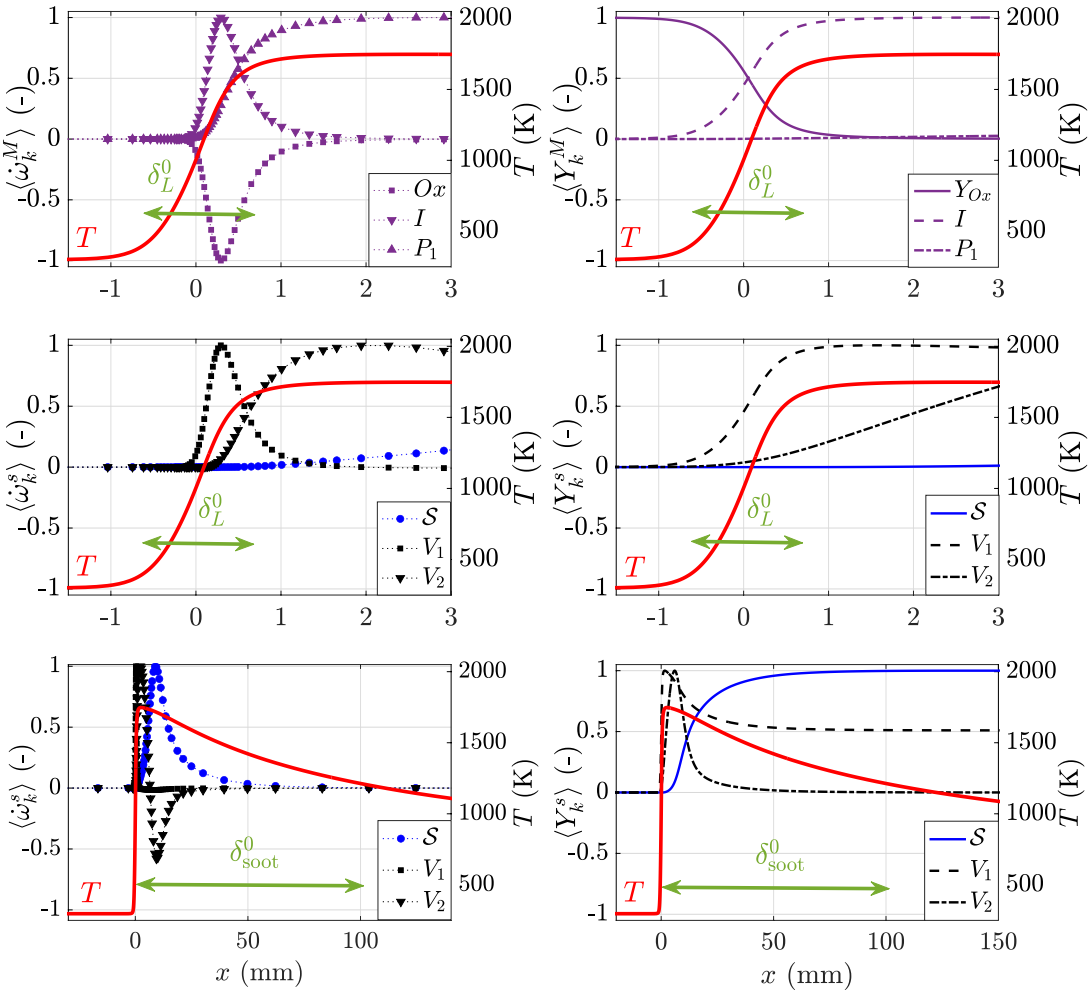

Figure 1: Laminar ethylene-air flame structure, $\phi = 2.4$. Top: Temperature T (solid red line), normalized source terms $\langle \dot{\omega}_k \rangle$ (symbols with dotted lines in left column), and normalized species mass fractions $\langle Y_k \rangle$ (lines in right column) profiles of the main mechanism; Middle and Bottom: values for the soot sub-mechanism. Normalization is defined as: $\langle \varphi \rangle = \varphi / \max(|\varphi|)$.

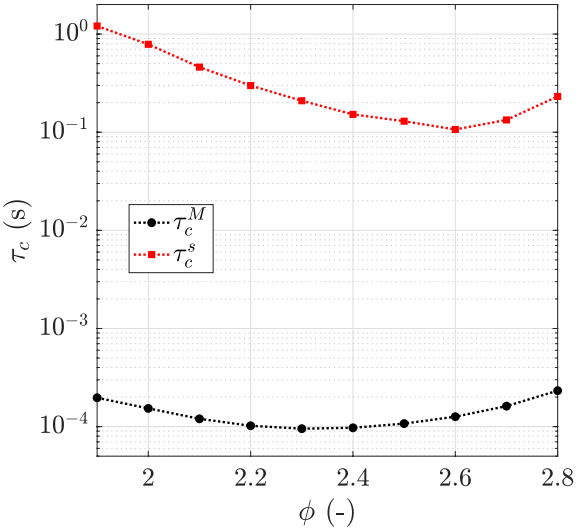

Figure 2: Chemical time scales associated with the flame front τ_c^M and the soot formation τ_c^s in 1-D laminar premixed ethylene-air flames for different equivalence ratios ϕ.

4.2. Soot subgrid-scale model

Turbulence interactions with the flame front and the post-flame reactive layers are characterized here by introducing the following subgrid-scale Damkhöler numbers:

$$\mathrm{Da}^M = \frac{\tau_t}{\tau_c^M}, \qquad \mathrm{Da}^s = \frac{\tau_t}{\tau_c^s}. \tag{8}$$

The turbulence time scale, $\tau_t = \Delta_x / u'_{sgs}$, is evaluated from the LES filter characteristic length Δ_x and the subgrid-scale (SGS) velocity fluctuation u'_{sgs}.

As shown in Fig. 2, chemical time scale involved in the flame front (main mechanism) is of the order of 10^{-4} s, which is expected to be smaller than the turbulence time scales encountered in practical combustion chambers. Consequently $\mathrm{Da}^M > 1$, and the flamelet regime is retrieved. As in the

classical TFLES approach [12], the filtered species reaction rates in Eq. 4 involved in the main mechanism are modeled with the subgrid-scale flame wrinkling Ξ_Δ:

$$\overline{\dot{\omega}}_k^M = \frac{\Xi_\Delta}{F_T}\dot{\omega}_k^M. \tag{9}$$

This approach is quite enough to resolve the turbulent-chemistry interactions in the flame front region and has been used in multiple occasions in practical turbulent combustion applications (to resolve for instance heat release and CO) [19, 25, 26]. However, the same closure cannot be retained for species involved in the current virtual soot sub-mechanism which involves both short and long time scales. The following hybrid formulation is therefore proposed to model $\overline{\dot{\omega}}_k^s$:

$$\overline{\dot{\omega}}_k^s = S_F \cdot \frac{\Xi_\Delta}{F_T}\dot{\omega}_k^s + (1 - S_F) \cdot \overline{\dot{\omega}}_k^s \Big|^{\text{PostFlame}} . \tag{10}$$

In the flame front region, S_F takes the value of unity, and Eq. 10 is then simplified to $\overline{\dot{\omega}}_k^s = \Xi_\Delta \dot{\omega}_k^s / F_T$ and flamelet regime assumption is retrieved. Recalling Eq. 4, the source term is activated together with the laminar diffusive term as adopted for the flamelet regime. At the opposite, in the post-flame region, $S_F = 0$, and the filtered reaction rate is given by $\overline{\dot{\omega}}_k^s \Big|^{\text{PostFlame}}$, and in Eq. 4, both laminar and turbulent diffusive terms are also triggered.

The model is written so that Eq. 4 degenerates towards a classical TFLES formalism at the flame front ($S_F = 1$) while no thickening is applied in the post-flame region ($S_F = 0$).

Now considering the soot sub-mechanism, the reaction R_1^s, which produces soot precursor V_1, is mainly effective at the flame front while reactions R_2^s through R_4^s act in the post-flame region. Therefore, in order to account

for the turbulent mixing, an efficiency factor η_r is introduced into the filtered soot reaction rate:

$$\overline{\dot{\omega}}_k^s \Big|^{\text{PostFlame}} = \sum_{r=1}^{N_r^s=4} \eta_r \ \alpha_{k,r}^s q_r^s. \tag{11}$$

At the post-flame region, the following features must be ensured:

- $S_F = 0$ should be guaranteed with the adequate main mechanism indicators [19],
- Rates of consumption of fuel (F) and oxidizer (Ox) should be consistent between main and soot mechanism (reactions R_1^s and R_1^M),
- The SGS turbulence-soot-chemistry interactions should be in concordance with the previous item.

Consequently for the first reaction in Eq. 11, one should have:

$$\eta_1 = \frac{\Xi_\Delta}{F_T}. \tag{12}$$

Soot characteristics time scales involved in reactions R_2^s through R_4^s are (primarily) expected to be slower than subgrid turbulent time scale. Therefore $\text{Da}^s << 1$ and the combustion regime at the SGS may be assimilated to perfectly-stirred reactor (PSR) regime [20]. The efficiency factor η_r is then modeled by the Damkhöler number as:

$$\eta_r = \max\left(\frac{1}{\text{Da}^s}, 1\right) \text{ for } r = 2, \text{ to } 4. \tag{13}$$

Turbulence will then enhance the combustion by a factor $1/\text{Da}^s$. When the turbulence vanishes at the subgrid-scale, *i.e.*, when the system behaves as

a laminar reacting flow, then $u'_{sgs} \rightarrow 0$, and according to Eq. 8 the soot Damköhler number $\mathrm{Da}^s \rightarrow +\infty$. Then, Eq. 13 ensures that $\eta_r \rightarrow 1$ and that the laminar flame regime is well recovered.

Prior to the 3-D calculations of the following Section, an analysis of the phenomenological behavior of 1-D pseudo-turbulent flames is performed, using the hybrid turbulent combustion model, which is included in Appendix A.

4.3. Radiation model

Sooting flames may present significant radiative heat losses. Therefore, the new virtual radiative model proposed by Maldonado Colmán et *al*. [6] is employed here. This model is able to produce the radiative effects of both gas and soot in hydrocarbon-air sooting flames. The radiative source term is modeled by optically-thin approximation:

$$\dot{Q}_r = 4\kappa^v_{\mathrm{Planck}}\sigma\left(T^4 - T_b^4\right), \tag{14}$$

where T_b is the background cold temperature, σ is the Stephan-Boltzmann constant and $\kappa^v_{\mathrm{Planck}}$ is the virtual Planck absorption coefficient. $\kappa^v_{\mathrm{Planck}}$ is composed of the contributions of gas and solid phases as $\kappa^v_{\mathrm{Planck}} = \kappa^M_{\mathrm{gas}} + \kappa^v_{\mathrm{soot}}$.

The gas absorption coefficient κ^M_{gas} is modeled as a fifth-order polynomial function of the inverse of the temperature, whose set of polynomial coefficients is optimized according to the methodology described in Ref. [6]. The learning database consists of 26 non-adiabatic premixed flames including gas radiation only based on Ref. [27] (ϕ ranging in $[0.5; 3.0]$). The set of gaseous Planck mean absorption parameters is optimized using the machine learning algorithm of Ref. [21], by comparing the results of temperature and laminar

flame speed against the learning database [6]. The set conducing to the best fitness compared to detailed chemistry results is finally selected [6].

The soot absorption coefficient κ^v_{soot} is proportional to the temperature T and the soot volume fraction f^s_v using the main and soot sub-mechanisms, respectively. The modeling constant is based on Ref. [28]. For further information about the virtual radiative model, we refer the reader to Ref. [6].

The filtered radiative source term is calculated by neglecting SGS temperature and composition fluctuations, using Eq. 14, as follows:

$$\overline{\dot{Q}}_r \simeq \dot{Q}_r(\widetilde{T}, \widetilde{Y}^v_k). \tag{15}$$

5. LES of a turbulent sooting flame

The experimental configuration retained for validation is the turbulent non-premixed ethylene-air jet flame, the Sandia burner [17], studied by the International Sooting Flame (ISF) workshop [29]. The burner consists of a central jet of pure ethylene with an inner diameter of $D = 3.2$ mm. The central jet is surrounded by a coflow of air and a pilot flame. The central jet bulk velocity is $u^{\text{bulk}}_{fuel} = 54.7\ \text{cm} \cdot \text{s}^{-1}$. The pilot flame is fed with a premixed ethylene-air mixture of $\phi = 0.9$ at a mass flowrate of $1.772 \times 10^{-4}\ \text{kg} \cdot \text{s}^{-1}$, corresponding to 2% of the heat release rate of the central jet. The air coflow mean velocity is $0.6\ \text{m} \cdot \text{s}^{-1}$. All gas flows are injected at atmospheric pressure and $T_0 = 294$ K. For further details on the experimental configuration, the reader may refer to [17].

5.1. Numerical setup

The computational domain has a cylindrical shape with a diameter of $188D$ and a length of $500D$. The unstructured grid is made of 43.4 millions

of tetrahedral cells. The smallest cells of length $\Delta_x \sim 0.1$ mm are located at the main jet exit.

No-slip condition is imposed at the injector walls. Fully-developed velocity profiles (including velocity fluctuations) issued from a pipe flow simulation is prescribed at the main inlet as in [30]. Uniform velocity profiles are assumed at the coflow and pilot inlets boundary conditions. Burnt gases at thermodynamic equilibrium, corresponding to the mixture previously mentioned, are injected at the pilot inlet. The pilot walls are non-adiabatic and a uniform temperature distribution of 1000 K is imposed. Other lateral walls are adiabatic.

The hybrid turbulent combustion model for soot from Section 3 and the models for turbulence-chemistry interactions and radiation developed in Section 4 are implemented in the low-Mach, unstructured finite-volume YALES2 code [31]. In this code, the convective terms are solved with a 4^{th} order scheme in time and space. The subgrid Reynolds stress tensor is closed using the sigma model [32]. The filtered radiative source term in the energy equation is approximated by using Eq. 15 and neglecting subgrid-scale temperature and mixture fraction fluctuations.

The SGS flame wrinkling Ξ_Δ is closed with the Charlette model [33, 34], with the constant parameter $\beta = 0.5$. A constant Prandtl number $\mathrm{Pr} = 0.7$ is considered. The Lewis number for virtual species is set to unity except for the virtual soot species $\mathcal{S}$, then Schmidt numbers are $\mathrm{Sc}_k = 0.7$, for k$\neq \mathcal{S}$. Indeed, according to [6], the Lewis number for the virtual soot species $\mathcal{S}$ is set to $\mathrm{Le}_\mathcal{S} = 25$, which corresponds to a laminar Schmidt number of $\mathrm{Sc}_\mathcal{S} = 17.5$. The turbulent Schmidt number of all virtual species, including

$\mathcal{S}$, is dynamically evaluated as in [35].

The time and Favre averaging for the statistics are accumulated over 250 ms of physical time (about 3.5 times the flow-through time on the flame length).

6. Results

Figure 3 gives a typical 2-D representation of instantaneous temperature (a) and soot volume fraction (b) using the virtual non-adiabatic model as mentioned above. The radiative heat losses decrease the peak temperature along the stoichiometric iso-line by 250 K.

As expected, the high concentration of soot is located in the fuel-rich region. The maximum soot volume fraction is about 1.6 ppm, which is similar to what is observed in the experiments [36].

6.1. Temperature and major species radial profiles

To highlight the importance of radiative effects in turbulent sooting flame simulation, both adiabatic and non-adiabatic simulations are performed. Figure 4 compares experimental and numerical radial profiles of the mean (top) and RMS (bottom) temperature at two axial locations x/D =134 and x/D =175. Adiabatic simulations significantly overestimate the temperature whereas non-adiabatic solutions are in good agreement with experimental data [37]. The non-adiabatic model gives less than 10% of discrepancy in the mean profiles.

Numerical RMS curves show differences up to 50% compared to experiments. However, RMS in simulation (*i.e.,* of the resolved field) are not directly comparable to the experimental RMS because subgrid fluctuations

are not taken into account [38]. The computation accuracy is comparable to results shown in [39], obtained by combining the RFPV turbulent combustion model [3] and a Monte Carlo radiative solver.

Further validation of the reacting mixture is now done by comparing X_{O_2}/X_{N_2} profiles of the LES results against experimental measurements [37]. Figure 5 presents the mean (top) and RMS (bottom) profiles of X_{O_2}/X_{N_2} for two different distances from the injector. At both position, mean profiles using the non-adiabatic model are in good agreement with experimental measurements, with an underestimation of about 25 %. Without radiation, the mixture profile is under predicted a bit more. Numerical results show that LES can qualitatively capture the RMS fluctuations but underestimates them by a factor of about 2 to 3 at $x/D = 134$ and lower than 30 % at $x/D = 175$.

6.2. Soot volume fraction profiles

Figure 6 compares mean (top) and RMS (bottom) radial profiles of soot volume fraction profiles at three axial positions. Numerical results using the adiabatic and non-adiabatic hybrid turbulent combustion model are compared to experimental data [17]. The non-adiabatic virtual chemistry model fairly reproduces the soot formation. Although the radial profiles meet correct orders of magnitude of soot volume fraction and the sooting region ($|r/D| \lesssim 15$) compared to the experimental measurements, other qualitative features such as the double-peak are not well captured. Nevertheless, it should be noted that results are in good rapport with other state-of-the-art numerical results [39, 40].

Figure 7 presents mean soot volume fraction along the burner axis. Adiabatic and non-adiabatic profiles obtained by the hybrid turbulent combustion

model are compared to experimental data of [17] and to three recent LES results from other groups involved in the ISF workshop. The various numerical strategies employed to model soot formation and corresponding references are indicated in Table 1. In Results #1, a tabulated chemistry was considered for the gas phase based on [41], a sectional method for soot formation with a lumped PAH for the nucleation model [30] and Monte Carlo method for radiation [39]. In Results #2 and #3, the tabulated chemistry was based on [42], the soot formation was modeled using a method of moments [43, 44] and optically thin approximation for radiation [27]. Both works [43, 44] consider PAH dimerization to couple the gas-solid transition, however in Results #2 a multiple species nucleation strategy is used, while a lumped PAH transport equation used in Results #3.

Regarding the turbulence-soot interactions, SGS models based on the work of Mueller and Pitsch [9, 45] are used for results #1, #2 and #3. The model from Results #3, however, took a further measure by adapting the soot SGS model to capture soot phenomena only in mixture compositions where soot growth rates are higher than the oxidation rate and, in this way, then the spurious soot oxidation is reduced [7]. Further information about the chemistry and soot models, the reader is referred to the references shown in Table 1.

The non-adiabatic hybrid turbulent combustion model predicts correctly maximum soot volume fraction, while neglecting the radiation effects causes a significant underprediction. Soot is however produced too fast by the hybrid turbulence-soot model while the consumption rate is fairly captured after the peak. Indeed, it should be noted that the building-up process of the hybrid

Results	Gas-phase chemistry	Soot model	Radiative Model	Reference
#1	Tabulated chemistry	Method of moment	Optically Thin	[40]
#2	Tabulated chemistry	Sectional model	Monte Carlo	[39]
#3	Tabulated chemistry	Method of moment	Optically Thin	[7]

Table 1: Modeling strategies of the simulation results shown in Fig. 7.

turbulent combustion model did not cover effects such as pyrolysis, gradual PAH formation, or another chemical path that could help capture this delay. In addition, the learning database does not cover the situation where soot convects towards the flame front, and soot growth in fuel-lean regions might be underpredicted as observed in a laminar non-smoking coflow flame [6]. Therefore, the learning database needs to be enlarged. However, this misprediction of soot region position was observed in other LES of turbulent jet flames in the literature using detailed combustion and soot models [45, 46].

Compared to the other numerical models, the virtual chemistry model is up to par with the state-of-the-art of this configuration. The maximum soot volume fraction is underpredicted by a half in Result #1 [40], and overpredicted by a factor greater than 2.5 in Results #2 [39] and #3 [7]. However, the position of the peak of soot volume fraction is only well predicted by Result #1 [40]. Result #3 [7] overestimates the peak position by $23D$, while Result #2 [39] and the hybrid turbulent combustion solution underestimate it by $16D$ and $58D$, respectively. In terms of computational costs, the LES using the virtual model required a total of about 2.2×10^5 CPU-hours to cover the 250 ms simulation time.

6.3. Effect of the soot SGS model

To highlight the influence of the hybrid combustion regime model, a simulation has been performed by neglecting the impact of the subgrid-turbulence on the soot chemistry in the post-flame region, *i.e.*, $\eta_r = 1$ for $r = 1$ to 4 in Eq. 11. Figure 8 compares the solution of this simulation against the hybrid model solution and experiments. A significant underestimation of f_v is revealed when the hybrid model is turned off (factor 3). Same effect on soot production in the Sandia burner was also observed in [7], where a difference of an order of magnitude is observed when changing the SGS model.

6.4. A posteriori validation

Figure 9 shows the scatter plot of Da^M and Da^s in the radial direction, at three horizontal planes located at $x/D = 9.375$, 31.25, 93.75 and 187.5 for the non-adiabatic simulation using the hybrid combustion regime model. The flame front chemistry is dominant at $x/D = 9.375$ while the soot chemistry starts further downstream at about 31.25 and is well established at $x/D = 93.75$. Soot consumption continues far downstream in the post-flame region, at $x/D = 187.5$, where the flame chemistry is completed. As anticipated in Section 2, Da^M is larger than unity, which is in accordance with the flamelet assumption retained to close the filtered reaction rates involved in the main mechanism. Conversely, Da^s is smaller than one for all axial positions.

An estimation of the resolved soot reaction layer is given by the following relationship:

$$\delta_{\mathcal{S}}^1 = \frac{1}{\max\{\mathrm{grad}\,\langle Y_{\mathcal{S}}^s \rangle\}} \ , \tag{16}$$

where $\langle Y_{\mathcal{S}}^s \rangle$ stands for the mean soot mass fraction. For instance, at $x/D = 101.6$: $\delta_{\mathcal{S}}^1 \approx 9$m. As expected, soot evolves at a scale much larger than the mesh size (here $\max \Delta_x \approx 2$mm) and there is no flame resolution issues in the post flame region.

These observations validates *a posteriori* the PSR model selected to close the filtered reaction rates related to soot virtual chemistry.

7. Conclusions and discussion

The virtual chemistry and radiative models developed for sooting laminar flames [6] have been implemented into an LES framework to simulate turbulent sooting flames. As soot chemistry exhibits a time scale much slower than the flame front chemistry, an original subgrid-scale hybrid reaction rate closure is proposed to cover both the flamelet regime chararacteristic of the thermal flame layer and a PSR-like regime observed in the post-flame region, where slow soot chemistry is dominant.

Three-dimensional LES of the Sandia burner is performed using the virtual chemistry, radiative and hybrid SGS models, giving good agreement with experimental measurements. The new virtual soot sub-mechanism captures well the soot physical phenomena and results are comparable to those of other groups obtained by using detailed models. The SGS model has a big impact on soot results, as observed by [7]. An analysis of the Damköhler numbers is performed *a posteriori* validating the closure for the filtered reaction rates related to soot virtual chemistry. In overall, soot-turbulent-chemistry interactions in the Sandia burner are fairly retrieved by the non-adiabatic hybrid approach.

Further modeling developments should however be considered to improve the results accuracy. This can be done at different levels by:

- enlarging the learning database target during the virtual chemical scheme optimization [22] in order to better capture the soot oxidation process;
- retaining a dynamic closure for the subgrid-scale flame wrinkling in the flame front region [47];
- introducing a more detailed closure in the distributed combustion regime encountered in the post-flame region [13, 14];
- *a priori* testing of turbulent source term closure against DNS data of a turbulent sooting reactive flow representative of post-flame conditions. Such comparison aims to challenge the modeling of the efficiency parameter η_r used in Eq. 13. The configuration will be similar to the one computed by Caudal *et al.* [48] to study turbulent chemistry interaction in partial oxidation processes.

Additional efforts are needed to assess the CPU cost required by each methodology shown in this paper. Estimating the costs by combining different approaches to solve the gas phase kinetics (tabulated, analytically reduced, global, and virtual mechanisms) and soot (MoM, sectional, virtual models) using the same computational resources will help the users in the decision-making process based on their applications.

Finally, it is worth noting that the proposed hybrid model can be used for the prediction of other pollutants whose chemical formation exhibits also both short and long characteristic time scales such as NOx.

Acknowledgments

Vincent Moureau and Ghislain Lartigue from CORIA laboratory and the SUCCESS scientific group are acknowledged for providing the YALES2 code. This work was granted access to the HPC resources of IDRIS and TGCC under the allocations A0112B10253 made available by GENCI (Grand Equipement National de Calcul Intensif), and HPC resources from the Mésocentre computing center of CentraleSupélec and Ecole Normale Supérieure Paris-Saclay supported by CNRS and Région Ile-de-France.

Appendix A. Analysis of the phenomenological behavior of 1-D pseudo-turbulent flames using the hybrid model

Prior to turbulent flame calculations, the new subgrid-scale (SGS) model using virtual chemistry is tested in 1-D pseudo-turbulent sooting flame simulations. The phenomenological behavior of the flames is analyzed in order to determine the contribution of the new hybrid model on the soot chemical source terms as depicted in Eq. 10.

The YALES2 code is employed to carry out the computations. 1-D premixed ethylene-air flames with equivalence ratio of $\phi = 2.5$ are simulated using the non-adiabatic virtual chemistry. In order to mimic the turbulent flame propagation speed, the inlet speed is set to 3 times the value of the laminar flame speed. The flames are artificially stabilized by setting the flame wrinkling factor equal to $\Xi_\Delta = 3$ so as the turbulent flame speed $S_T = \Xi_\Delta S_L^0$ [20], with $S_L^0(\phi = 2.5) = 0.113\,\mathrm{m/s}$. Then, two cases are considered to resolve the flames, on a coarse grid with uniform element size of $\Delta_x = 0.5\,\mathrm{mm}$, as follows:

1. An artificially thickened flame with thickening factor equal to $T_F = 5$, referred to as the "Flamelet" case. The impact of the subgrid-turbulence on the soot chemistry in the post-flame region is neglected: *i.e.*, $\eta_r = 1$ for $r = 1$ to 4 in Eq. 11.
2. An artificially thickened flame with thickening factor equal to $T_F = 5$ including the new hybrid turbulent combustion model of Section 4, simply referred to as the "PSR" case. Three simulations are conducted by imposing constant values for the efficiency: $\eta = 1.1$, 1.5, and 2

Results plotted in Fig. A.1, show the temperature (left), soot volume fraction (center), and soot source terms (right) profiles of the 1-D pseudo-turbulent flames. As expected, the temperature profile is not impacted by the soot SGS closure. However significant differences are observed on the soot production in the post-flame region, for $x > 10\,\mathrm{mm}$: the soot volume fraction is enhanced when the efficiency η increases. This is also evidenced in Fig. A.1 (right), which shows soot source term normalized as:

$$\langle \dot{\omega}_{\mathcal{S}}^{s} \rangle_{\mathrm{Flamelet}} = \frac{\dot{\omega}_{\mathcal{S}}^{s}|_{\mathrm{PSR}}}{\max\left(\dot{\omega}_{\mathcal{S}}^{s}|_{\mathrm{Flamelet}}\right)}. \tag{A.1}$$

The contribution of the soot source term in the flame front is negligible compared to that of the post-flame (see solid lines in zoomed subfigure), with a difference of about two orders of magnitude. Since the soot source term is significant at about 10mm away from the flame front, there is no considerable impact from the thickening and wrinkling operations. This confirms the hypothesis made to establish the hybrid flamelet-PSR model presented in Section 4.

References

[1] M. Frenklach, H. Wang, Detailed mechanism and modeling of soot particle formation, H. Bockhorn (Ed.), Soot Formation in Combustion: Mechanisms and Models (New York, 1994).

[2] O. Gicquel, N. Darabiha, D. Thévenin, Laminar premixed hydrogen / air counterflow flame simulations using flame prolongation of ILDM with differential diffusion, Proc. Combust. Inst. 28 (2000) 1901–1908.

[3] M. Ihme, H. Pitsch, Modeling of radiation and nitric oxide formation in turbulent nonpremixed flames using a flamelet/progress variable formulation, Phys. Fluids 20 (2008) 055110.

[4] P. Pepiot, Automatic strategies to model transportation fuel surrogates, Ph.D. thesis, Stanford University, 2008.

[5] B. Franzelli, E. Riber, M. Sanjosé, T. Poinsot, A two-step chemical scheme for kerosene-air premixed flames, Combust. Flame 157 (2010) 1364 – 1373.

[6] H. Maldonado Colmán, A. Cuoci, N. Darabiha, B. Fiorina, A virtual chemistry model for soot prediction in flames including radiative heat transfer, Combust. Flame 238 (2022) 111879.

[7] S. Yang, J. K. Lew, M. E. Mueller, Large eddy simulation of soot evolution in turbulent reacting flows: Presumed subfilter PDF model for soot-turbulence-chemistry interactions, Combust. Flame 209 (2019) 200 – 213.

[8] H. El-Asrag, T. Lu, C. K. Law, S. Menon, Simulation of soot formation in turbulent premixed flames, Combust. Flame 150 (2007) 108–126.

[9] M. E. Mueller, H. Pitsch, Large eddy simulation subfilter modeling of soot-turbulence interactions, Phys. Fluids 23 (2011) 115104.

[10] L. Berger, A. Wick, A. Attili, M. E. Mueller, H. Pitsch, Modeling subfilter soot-turbulence interactions in Large Eddy Simulation: An a priori study, Proc. Combust. Inst. 38 (2021) 2783–2790.

[11] N. Peters, Laminar flamelet concepts in turbulent combustion, Symp. (Int.) Combust. 21 (1988) 1231–1250.

[12] B. Fiorina, D. Veynante, S. Candel, Modeling combustion chemistry in large eddy simulation of turbulent flames, Flow Turbul. Combust. 94 (2015) 3–42.

[13] Z. Li, A. Cuoci, A. Parente, Large eddy simulation of mild combustion using finite rate chemistry: Effect of combustion sub-grid closure, Proc. Combust. Inst. 37 (2019) 4519–4529.

[14] E. Fooladgar, P. Toth, C. Duwig, Characterization of flameless combustion in a model gas turbine combustor using a novel post-processing tool, Combust. Flame 204 (2019) 356–367.

[15] Z. Huo, M. J. Cleary, A. R. Masri, M. E. Mueller, A coupled mmc-les and sectional kinetic scheme for soot formation in a turbulent flame, Combustion and Flame 241 (2022) 112089.

[16] B. Sun, S. Rigopoulos, Modelling of soot formation and aggregation in turbulent flows with the les-pbe-pdf approach and a conservative sectional method, Combustion and Flame 242 (2022) 112152.

[17] J. Zhang, C. R. Shaddix, R. W. Schefer, Design of "model-friendly" turbulent non-premixed jet burners for C2+ hydrocarbon fuels., Rev Sci Instrum 82 (2011) 074101.

[18] J.-P. Legier, T. Poinsot, D. Veynante, Dynamically thickened flame LES model for premixed and non-premixed turbulent combustion, in: Proceedings of the Summer Program, volume 2000, Center for Turbulence Research Stanford, CA, 2000, pp. 157–168.

[19] M. Cailler, R. Mercier, V. Moureau, N. Darabiha, B. Fiorina, Prediction of CO emissions in LES of turbulent stratified combustion using virtual chemistry, in: 55th AIAA Aerospace Sciences Meeting Grapevine, Texas, USA, AIAA, AIAA paper 2017-1471, 2017.

[20] T. Poinsot, D. Veynante, Theoretical and numerical combustion, Third Edition by T. Poinsot, 2012.

[21] M. Cailler, N. Darabiha, D. Veynante, B. Fiorina, Building-up virtual optimized mechanism for flame modeling, Proc. Combust. Inst. 36 (2017) 1251 – 1258.

[22] M. Cailler, N. Darabiha, B. Fiorina, Development of a virtual optimized chemistry method. Application to hydrocarbon/air combustion, Combust. Flame 211 (2020) 281 – 302.

[23] G. Maio, M. Cailler, A. Cuoci, B. Fiorina, A virtual chemical mechanism for prediction of NO emissions from flames, Combust. Theory Model. 24 (2020) 872–902.

[24] C. Saggese, S. Ferrario, J. Camacho, A. Cuoci, A. Frassoldati, E. Ranzi, H. Wang, T. Faravelli, Kinetic modeling of particle size distribution of soot in a premixed burner-stabilized stagnation ethylene flame, Combust. Flame 162 (2015) 3356–3369.

[25] G. Maio, M. Cailler, R. Mercier, B. Fiorina, Virtual chemistry for temperature and CO prediction in LES of non-adiabatic turbulent flames, Proc. Combust. Inst. 37 (2019) 2591 – 2599.

[26] G. Maio, M. Cailler, N. Darabiha, B. Fiorina, Capturing multi-regime combustion in turbulent flames with a virtual chemistry approach, Proc. Combust. Inst. (2020).

[27] R. Barlow, A. Karpetis, J. Frank, J.-Y. Chen, Scalar profiles and no formation in laminar opposed-flow partially premixed methane/air flames, Combust. Flame 127 (2001) 2102–2118.

[28] M. F. Modest, Radiative Heat Transfer (Third Edition), Academic Press, Boston, 2013.

[29] ISF5, International sooting flame workshop, http://www.adelaide.edu.au/cet/isfworkshop/data-sets/, 2020.

[30] P. Rodrigues, B. Franzelli, R. Vicquelin, O. Gicquel, N. Darabiha, Coupling an LES approach and a soot sectional model for the study of soot-

ing turbulent non-premixed flames, Combust. Flame 190 (2018) 477 – 499.

[31] V. Moureau, P. Domingo, L. Vervisch, Design of a massively parallel cfd code for complex geometries, Comptes Rendus Mécanique 339 (2011) 141–148.

[32] F. Nicoud, H. B. Toda, O. Cabrit, S. Bose, J. Lee, Using singular values to build a subgrid-scale model for large eddy simulations, Phys. Fluids 23 (2011).

[33] F. Charlette, C. Meneveau, D. Veynante, A power-law flame wrinkling model for LES of premixed turbulent combustion part I: non-dynamic formulation and initial tests, Combust. Flame 131 (2002) 159–180.

[34] F. Charlette, C. Meneveau, D. Veynante, A power-law flame wrinkling model for LES of premixed turbulent combustion part II: dynamic formulation, Combust. Flame 131 (2002) 181–197.

[35] P. Moin, K. Squires, W. Cabot, S. Lee, A dynamic subgrid-scale model for compressible turbulence and scalar transport, Phys. Fluid Fluid Dynam. 3 (1991) 2746–2757.

[36] C. R. Shaddix, J. Zhang, R. W. Schefer, J. Doom, J. C. Oefelein, S. Kook, L. M. Pickett, H. Wang, Understanding and predicting soot generation in turbulent non-premixed jet flames, Sand2010-7178, Sandia Report (2010).

[37] S. P. Kearney, D. R. Guildenbecher, C. Winters, P. A. Farias, T. W.

Grasser, J. C. Hewson, Temperature, Oxygen, and Soot-Volume-Fraction Measurements in a Turbulent C2H4-Fueled Jet Flame, Technical Report SAND2015-7968, Sandia National Lab.(SNL-NM), Albuquerque, NM (United States), 2015.

[38] D. Veynante, R. Knikker, Comparison between les results and experimental data in reacting flows, Journal of turbulence 7 (2006) N35.

[39] P. Rodrigues, O. Gicquel, B. Franzelli, N. Darabiha, R. Vicquelin, Analysis of radiative transfer in a turbulent sooting jet flame using a monte carlo method coupled to large eddy simulation, J. Quant. Spectrosc. Radiat. Transf. 235 (2019) 187–203.

[40] A. Jain, Y. Xuan, Effects of large aromatic precursors on soot formation in turbulent non-premixed sooting jet flames, Combust. Theory Model. 23 (2019) 439–466.

[41] Y. Wang, A. Raj, S. H. Chung, A PAH growth mechanism and synergistic effect on pah formation in counterflow diffusion flames, Combust. Flame 160 (2013) 1667 – 1676.

[42] K. Narayanaswamy, G. Blanquart, H. Pitsch, A consistent chemical mechanism for oxidation of substituted aromatic species, Combust. Flame 157 (2010) 1879–1898.

[43] G. Blanquart, H. Pitsch, Analyzing the effects of temperature on soot formation with a joint volume-surface-hydrogen model, Combust. Flame 156 (2009) 1614 – 1626.

[44] M. E. Mueller, G. Blanquart, H. Pitsch, A joint volume-surface model of soot aggregation with the method of moments, Proc. Combust. Inst. 32 (2009) 785 – 792.

[45] M. E. Mueller, H. Pitsch, LES model for sooting turbulent nonpremixed flames, Combust. Flame 159 (2012) 2166 – 2180.

[46] F. Sewerin, S. Rigopoulos, An les-pbe-pdf approach for predicting the soot particle size distribution in turbulent flames, Combust. Flame 189 (2018) 62–76.

[47] G. Wang, M. Boileau, D. Veynante, Implementation of a dynamic thickened flame model for large eddy simulations of turbulent premixed combustion, Combust. Flame 158 (2011) 2199–2213.

[48] J. Caudal, B. Fiorina, B. Labégorre, O. Gicquel, Modeling interactions between chemistry and turbulence for simulations of partial oxidation processes, Fuel Process. Technol. 134 (2015) 231–242.

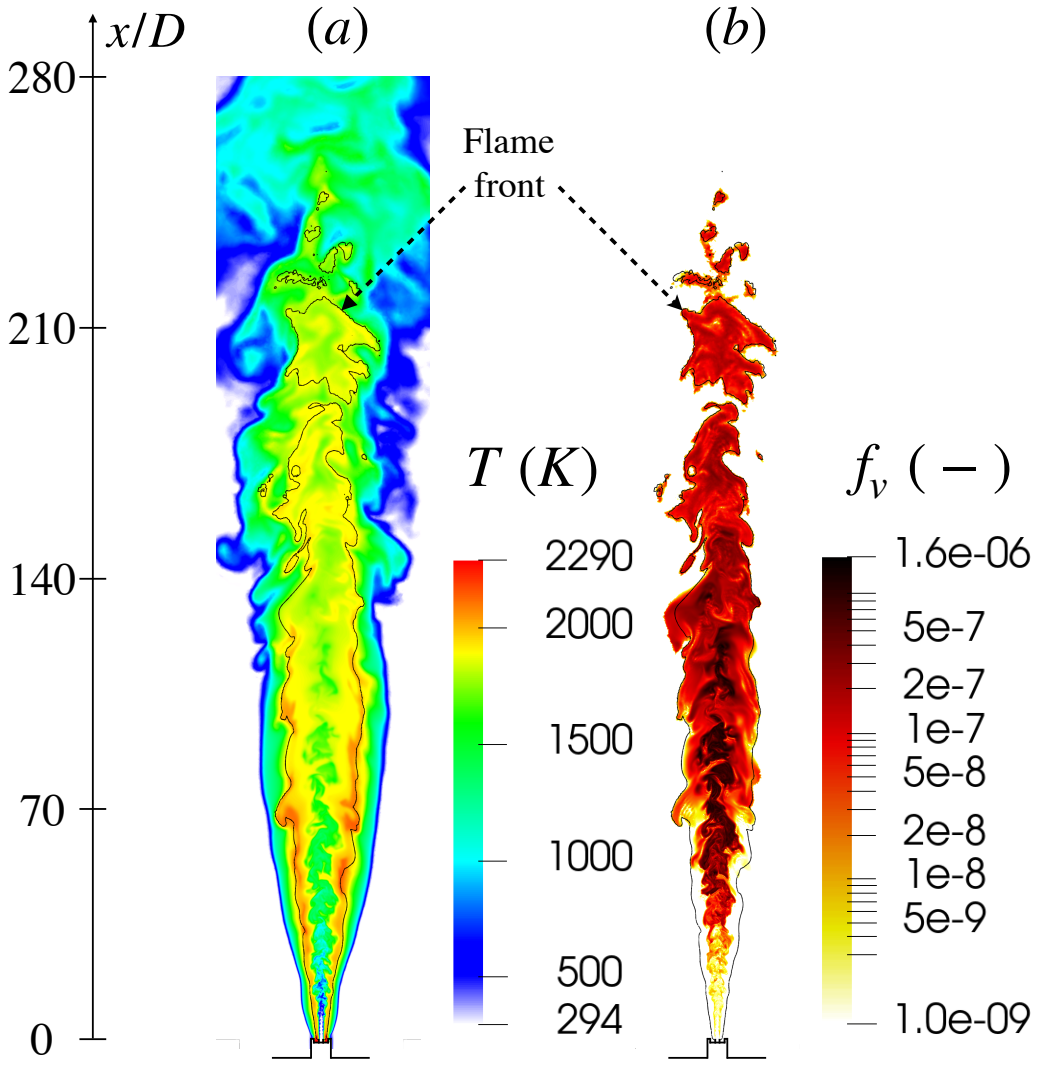

Figure 3: Instantaneous fields of (a) temperature and (b) soot volume fraction. The black continuous line on each figure corresponds to the stoichiometric mixture fraction Z_{st} indicating the flame front.

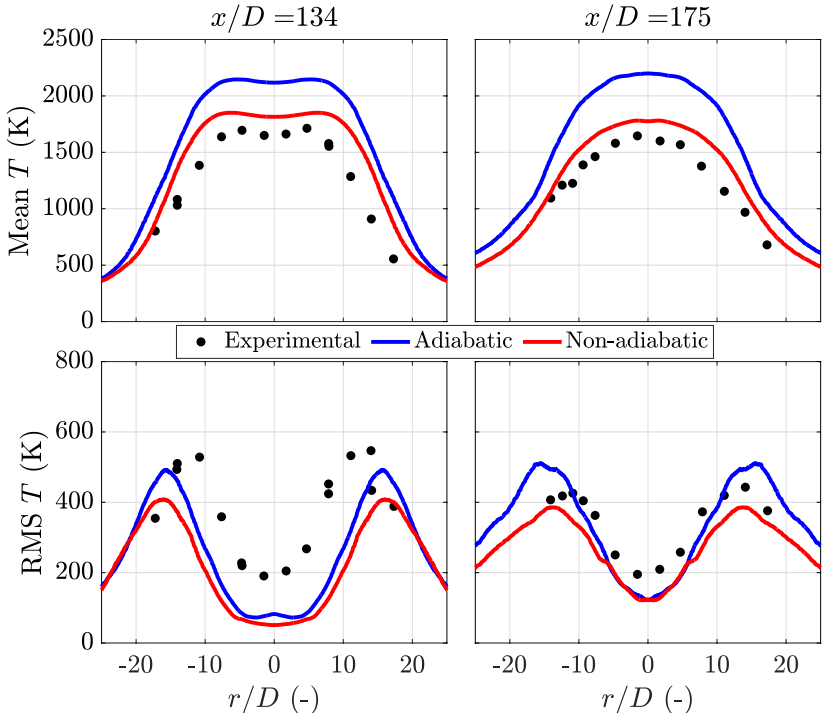

Figure 4: Radial profiles of mean (top) and RMS (bottom) temperatures at $x/D = 134$ (left) and $x/D = 175$ (right). Numerical results of adiabatic (blue) and non-adiabatic (red) cases are compared to experimental data (symbols) [37].

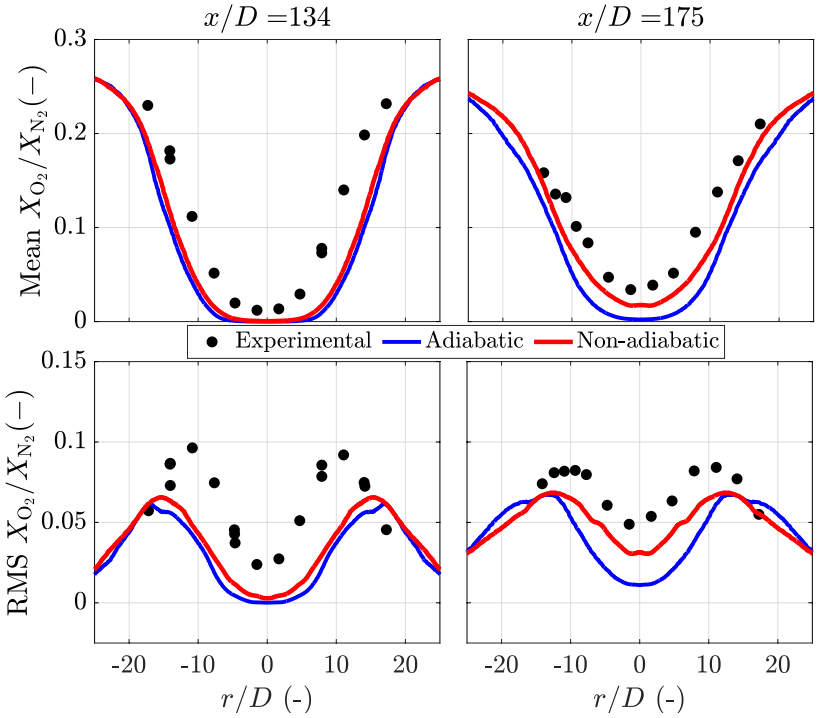

Figure 5: Radial profiles of mean (top) and RMS (bottom) X_{O_2}/X_{N_2} at $x/D = 134$ (left) and $x/D = 175$. Numerical results of adiabatic (blue) and non-adiabatic (red) cases are compared to experimental data (symbols) [37].

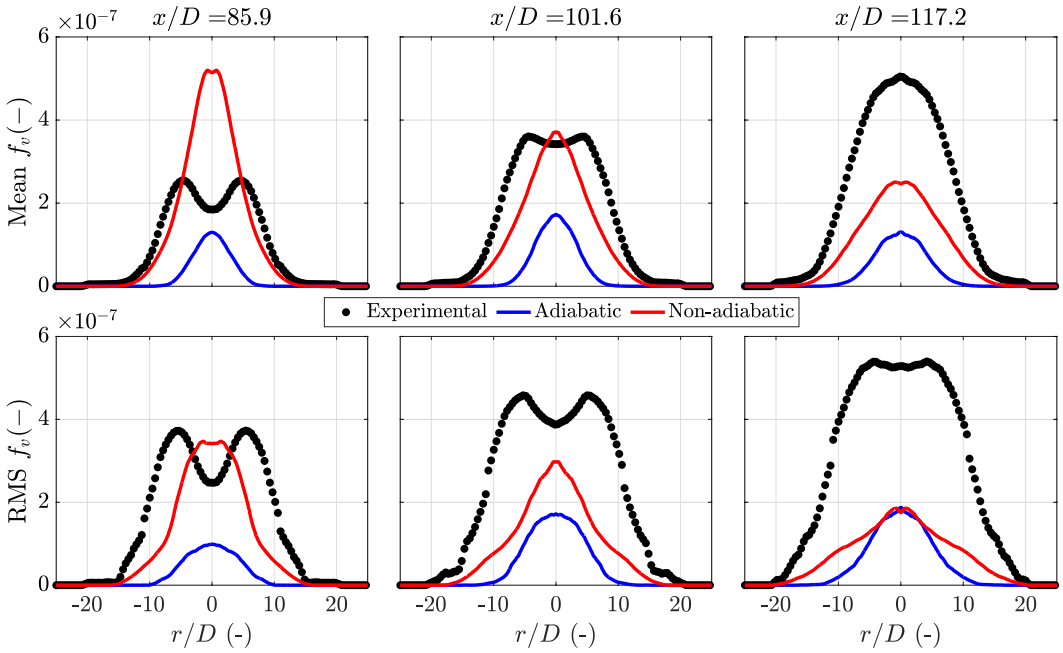

Figure 6: Radial profiles of mean (top) and RMS (bottom) soot volume fraction at three different axial positions x/D. Numerical results of the adiabatic (blue) and non-adiabatic (red) hybrid model are compared to experimental data (symbols) [17].

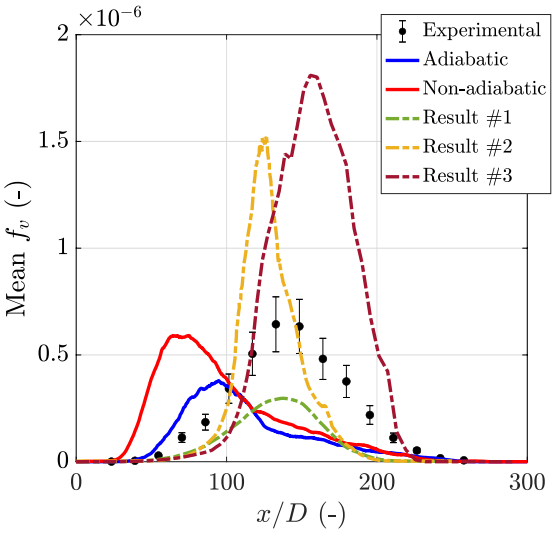

Figure 7: Mean soot volume fraction profile along the burner axis. See Table 1 for information about Results #1-3.

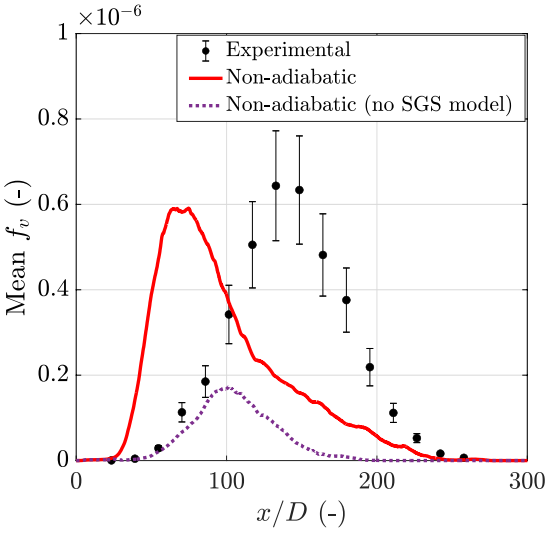

Figure 8: Mean soot volume fraction profile along the burner axis. Effect of the SGS model on soot formation.

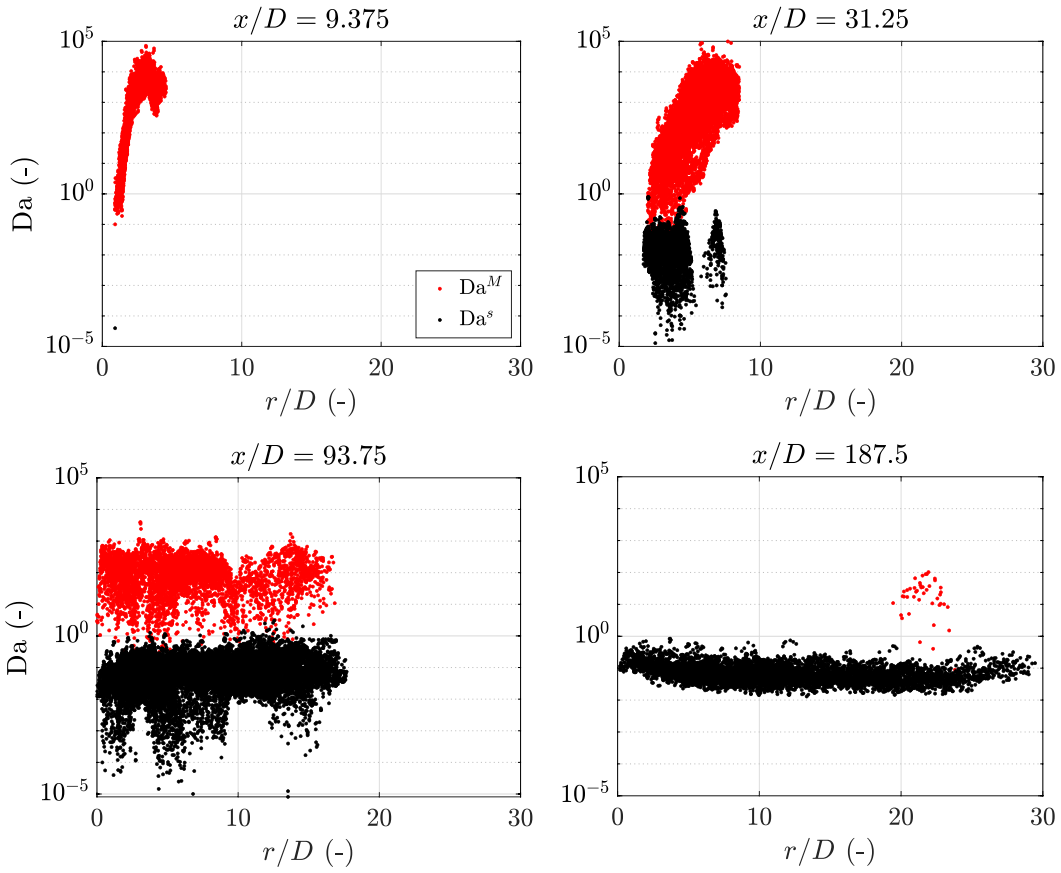

Figure 9: Scatter plot of flame (red) and soot (black) Damköhler numbers in the radial direction at a horizontal section y-z for four axial positions $x/D = 9.375$, 31.25, 93.75 and 187.5. Da^M is conditioned into the flame front region ($S_F = 1$), and Da^s outside the reaction zone ($S_F = 0$).

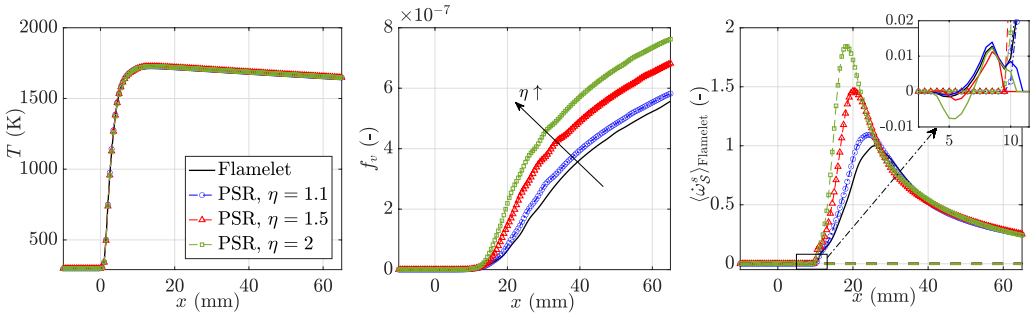

Figure A.1: Temperature (left), soot volume fraction (center), and normalized soot source terms (right) profiles of 1-D seudo-turbulent premixed ethylene-air flames with equivalence ratio $\phi = 2.5$: comparison of numerical results using the Flamelet and PSR models. The soot source terms are normalized following Eq. A.1, and separated by their contributions in the flame front (solid lines) and the post-flame (dashed lines with symbols) regions according to Eq. 10.